P15R.3

THE EVOLUTION OF A TORNADO: GROUND-BASED VELOCITY TRACK DISPLAY (GBVTD) ANALYSIS OF MOBILE, W-BAND, DOPPLER RADAR DATA ON 15 MAY 1999 NEAR STOCKTON, KANSAS

Robin L. Tanamachi*
Howard B. Bluestein
School of Meteorology, University of Oklahoma, Norman, Oklahoma

Michael Bell
Wen-Chau Lee
National Center for Atmospheric Research (NCAR), Colorado State University, Boulder, Colorado

Andrew L. Pazmany
ProSensing, Amherst, Massachusetts

Christopher C. Weiss
Atmospheric Science Group, Texas Tech University, Lubbock, Texas

1. INTRODUCTION

A tornado is characterized by short horizontal scale and rapid evolution. Deduction of the horizontal wind field in and around a tornado remains a formidable task. Detailed understanding of tornado vortex structure is critical for the improvement of safeguard mechanisms for life and property. In this study, the Ground Based Velocity Track Display (GBVTD) technique developed by Lee *et al.* (1999) is used to analyze the two-dimensional wind field from data recorded by a high-resolution Doppler radar in the vicinity of a tornado.

Fig. 1. The U. Mass. W-band radar collecting data in the Stockton, Kansas tornado on 15 May 1999. View to the northwest. Photograph © H. Bluestein.

* *Corresponding author address:* Robin L. Tanamachi; Univ. of Oklahoma, School of Meteorology; 100 E. Boyd, Rm. 1310; Norman, OK 73019; e-mail: rtanamachi@ou.edu .

2. THE STOCKTON TORNADO

On 15 May 1999, during a University of Oklahoma storm intercept mission, high-resolution radar reflectivity and velocity data were collected from several minutes after tornadogenesis up until the end of the life of a tornado near Stockton, Kansas (hereafter the "Stockton tornado"; see Fig. 1).

The Stockton tornado occurred in an isolated thunderstorm that developed over Rooks County, Kansas at approximately 19:20 CDT. Tornadogenesis occurred around 19:55:12 CDT. During the organizing stage of the life cycle of the tornado, which lasted approximately two minutes, the condensation funnel had a "ragged" appearance. The tornado exhibited a multiple-vortex structure over a period of approximately 75 seconds starting at around 19:55:30 CDT. The appearance of the tornado then changed to a classic "wedge" shape that was maintained for the next eight minutes (the mature stage). In the final two minutes (the decaying stage) of its life cycle, the condensation funnel became thinner and vaguely helical in appearance, before dissipating altogether at 20:06:07 CDT. In general, no multiple vortices were visible during the mature or decaying stages of the life cycle of the Stockton tornado.

3. W-BAND RADAR DATA

The Doppler radar data used in this study were collected by a mobile, 3 mm wavelength, 95 GHz (W-band), pulsed Doppler radar built by the University of Massachusetts (U. Mass) Microwave Remote Sensing Laboratory (Bluestein *et al.* 1995, 2004; hereafter "the W-band radar"). The W-band radar antenna has a half-power beamwidth of 0.18° and its transmitter has a selectable pulse length of 15 m or 30 m. The W-band radar transmitter implements a polarization diversity pulse pair (PDPP) technique (Doviak and Sirmans 1973) that increases its maximum unambiguous velocity from ±12 m s^{-1} to ±79 m s^{-1} (Pazmany *et al.* 1999).

Thirty-five sector scans were obtained by the W-band radar between 19:56:19 CDT and 20:06:07 CDT, documenting the mature and dissipating stages of the tornado. The time interval between scans was approximately 15 seconds, except for an interval of approximately two minutes (20:00:55 – 20:03:01 CDT) in which no scans were collected. The pulse length of the W-band radar was set to 30 m. The W-band radar was stationary throughout the collection period, during which the distance to the tornado, which tracked to north-northwest, increased from 4.5 km to 6.8 km (Fig. 2).

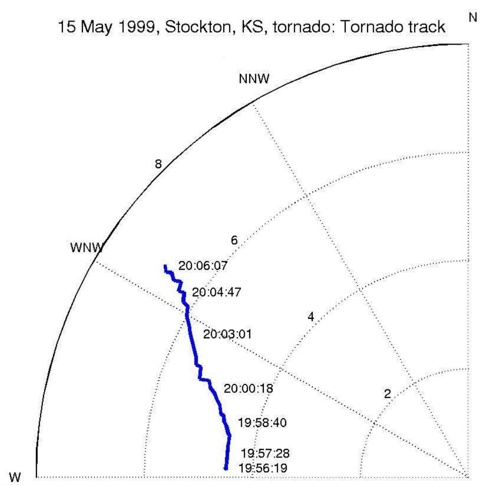

Fig. 2. Track of the Stockton tornado in polar coordinates. The W-band radar was located at the origin, facing east. Range rings are in km, times are in CDT (UTC – 5 hours).

Significant changes in the structure of the Stockton tornado at various stages of its life cycle were observed visually (as described in Section 2) and inferred from the radar data. Throughout the duration of the deployment, the tornado was characterized by one or more annuli of relatively high reflectivity, and was connected to the parent storm by an "umbilical cord" of high reflectivity, likely a rain curtain (Fig. 3). In the first 11 scans (covering the time interval from 19:56:19 to 19:58:26 CDT), the tornado was characterized by an annulus of relatively high reflectivity (4 to 8 dBZ_e) around its center, and possibly a second annulus of moderate reflectivity (-10 to -5 dBZ_e) surrounding the inner high-reflectivity annulus (Fig. 3a). In later scans (12 scans, covering the time interval from 20:00:55 to 20:05:03 CDT), the tornado was characterized by a double annulus of relatively high reflectivity (-5 to -1 dBZ_e, Fig. 4a). During the time interval between these visually distinct characters, the reflectivity structure of the tornado (not shown) underwent a transition that can be described as "unraveling": high-reflectivity filaments departed the inner high-reflectivity annulus, moved radially outward away from the center of the vortex, and formed a second, outer high-reflectivity annulus.

The low-reflectivity "eye" in the center of the tornado, probably formed by the centrifuging of water droplets and debris outward from the vortex center at the level of the radar scan (Dowell *et al.* 2005), also exhibited significant variations in reflectivity structure throughout the course of the data collection. The eye underwent several "pulses" in which its width, as measured by the diametric distance between maximum negative gradients of reflectivity near the vortex center, increased and decreased in an arrhythmic fashion (Fig. 5).

It should be noted that the truck, while very close to being level, was not *exactly* level with respect to the plane of the ground. Additionally, the boresighted video camera installed on the radar dish, which is used by the radar operator to direct the radar beam, provided video feed to the radar operator, but this video feed was not recorded because the video cassette recorder malfunctioned. The radar operator indicated that he attempted to direct the radar beam approximately halfway between the cloud base and the ground as seen in the video feed (A. Pazmany 2004, personal communication).

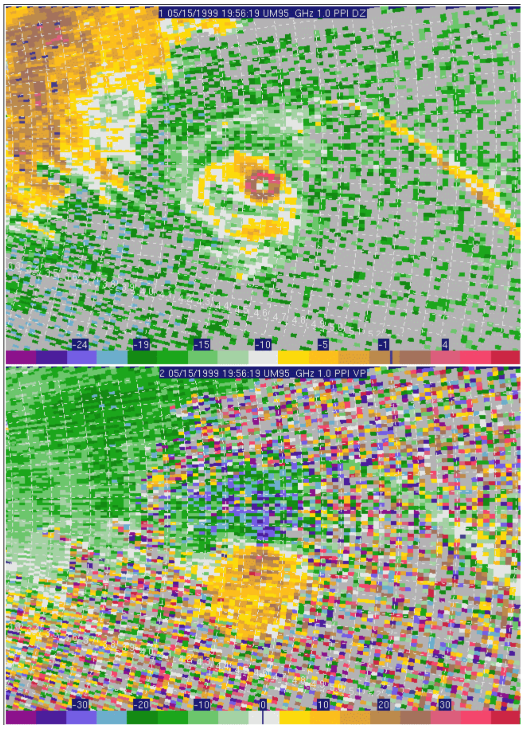

Fig. 3. W-band reflectivity (top) and Doppler velocity in dBZ (bottom) for the 15 May 1999 Stockton, KS tornado at 19:56:19 CDT. The azimuthal grid spacing is 1° and the radial grid spacing is 0.1 km. Because the radar was facing west, the coordinate system appears inverted.

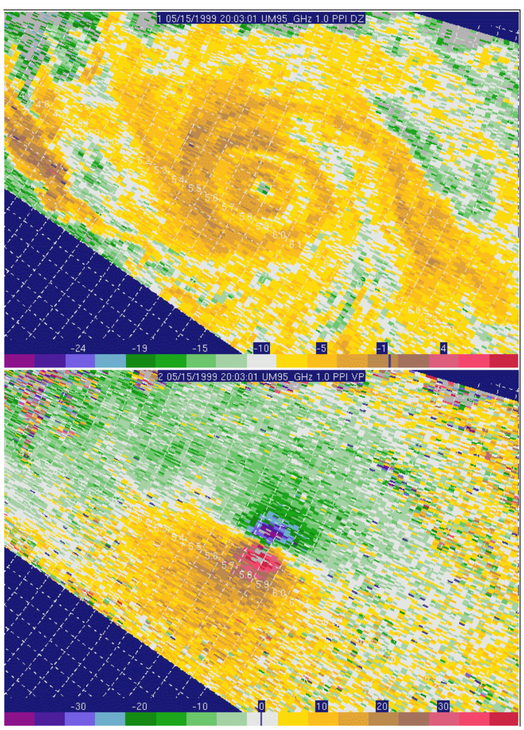

Fig. 4. Same as Fig. 3, but at 20:03:01 CDT, when the tornado was most intense, showing the "double annulus" structure that the tornado exhibited during later stages of its life cycle.

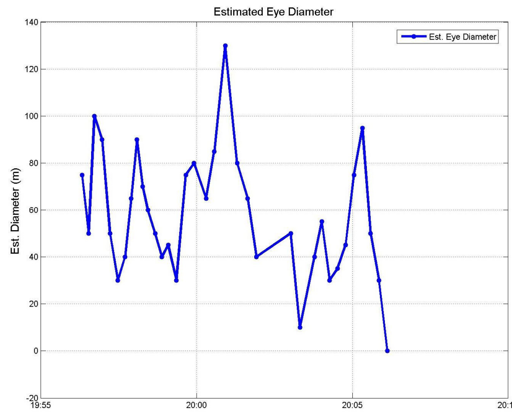

Fig. 5. Estimated diameter (in m) of the low-reflectivity "eye" of the Stockton tornado as a function of time.

A video recording was obtained of the W-band radar deployment and the tornado from a location approximately 30 m from the W-band radar deployment site. A photogrammetric analysis of this video of the Stockton tornado, coupled with still 35 mm slides (obtained by the second author) that were matched to frames in the video (not shown), yielded an estimated scan height of 90 m ± 10 m at a range of 4.5 km from the radar truck, and 125 m ± 15 m at a range of 6.2 km. These estimated heights correspond to an estimated radar elevation angle of 1.1 ± 0.2°. The plane of the radar scan can therefore be assumed to be quasi-horizontal and the vertical component of motion contained within the measured along-beam component of the Doppler velocity is insignificant in comparison with the horizontal component.

4. APPLICATION OF THE GBVTD TECHNIQUE

The highly axisymmetric structure of the Stockton tornado at the level of the radar scan made the W-band radar dataset collected in the Stockton tornado an excellent candidate for application of GBVTD analysis. The Ground-Based Velocity Track Display (GBVTD) technique is used to compute vortex-centered azimuthal and radial winds from a velocity data set taken by a single Doppler radar whose location is not coincident with the center of the vortex. The GBVTD technique is a ground-based adaptation of the velocity track display (VTD) technique used on tropical cyclone radar data taken by an airborne radar (Lee *et al.* 1994).

The GBVTD technique is based upon the assumption that an axisymmetric vortex exists within the sector, so that the Fourier transform of single Doppler velocities around the vortex center can be used to deduce the radial and tangential wind components of the vortex. The reader is referred to Lee *et al.* (1999) and Lee and Marks (2000) for a more detailed description of the GBVTD technique. The GBVTD technique has been applied to radar data in order to ascertain information about the kinematic structure of tropical cyclones (Lee *et al.* 2000) and tornadic vortices previously (Bluestein *et al.* 2003; Lee and Wurman 2005).

Some pre-processing of the W-band radar data was required in order to facilitate the application of the GBVTD analysis technique. The low-reflectivity eye often contained highly "speckled" velocity data because there were relatively few scatterers within. The GBVTD analysis, particularly the simplex center-seeking algorithm, is somewhat sensitive to erroneous Doppler velocity data. In order to reduce the effects of such data on the GBVTD analysis, a reflectivity threshold was applied to the velocity data, using National Center for Atmospheric Research SOLO II radar data processing software (Oye *et al*. 1995). Any velocity data point associated with a reflectivity data point recorded as -18 dBZe or less was ignored, as the velocity data from such points were considered suspect. A few additional velocity data points that were subjectively judged to be suspect (i.e. recorded rays in which the radar beam seemed to be blocked by a utility pole or other stationary obstruction) were also manually removed.

Successful application of the GBVTD technique requires that the aspect ratio between the radius of the tornado and the distance from the radar to the tornado not be excessively large, i.e., that the vortex not be located too close to the radar. When the distance between the radar and the tornado is less than or equal to the core radius of the tornado itself, the Doppler signature of the tornado becomes too distorted for accurate analysis (Wood and Brown 1992, 1997). The characteristics of the W-band radar dataset collected in the Stockton tornado satisfied the requirement that the aspect ratio was small, and that the data locations in radial and azimuthal space could be approximated as a Cartesian grid (Lee *et al*. 1999; Bluestein *et al*. 2003). The ratio of radial to azimuthal resolution for this dataset was on the same order of magnitude as that from Lee *et al*. (2000), in which a WSR-88D radar collected data in a typhoon.

Analysis of the 15 June 1999 Stockton, Kansas tornado radar dataset using the GBVTD technique involved three main procedures:

1. The reflectivity and velocity data from each of the thirty-five sector scans were remapped from their recorded plan position indicator (PPI) grid in radar-centered polar coordinates (degrees and kilometers) to a constant altitude PPI (CAPPI) Cartesian coordinate grid with a grid spacing of 20 m. (The change in scan level height with distance over the 150-m diameter of the tornado, which was approximately 3 m, was neglected.) The 20 m grid spacing was selected as a compromise between the radial resolution of the W-band radar (30 m) and its azimuthal resolution (15 m – 20 m) at the range of the Stockton tornado (4.5 – 6.2 km).
2. The center of the tornado vortex on the CAPPI grid was computed using the simplex vortex center-seeking algorithm of Lee and Marks (2000).
3. The winds around the vortex center found in the previous step were computed using the ground-based velocity-track display (GBVTD) analysis technique.

In the final procedure, the radar data were also transferred into a vortex-centered coordinate system, and the azimuthal winds were decomposed into azimuthally averaged wavenumber-0, -1, -2, and -3 angular harmonic components, as well as radial wind components, in 14 concentric annuli of 20 m thickness around the vortex center.

5. RESULTS

The application of the GBVTD technique to the 15 May 1999 Stockton, Kansas U. Mass. W-band radar data set yielded a set of GBVTD analyses of the two-dimensional wind field output for all thirty-five sector scans. An example is shown in Fig. 6. Azimuthally averaged velocities, reflectivity, circulation, vorticity, and divergence were also calculated as a function of radius for each scan. An example is shown in Fig. 7. By comparing GBVTD-analyzed azimuthally averaged azimuthal and radial velocities to the Doppler-measured velocities across the tornado at constant radius and Doppler-measured velocities across the tornado at constant azimuth, respectively, the quality of the GBVTD-analyzed azimuthally averaged azimuthal velocities were subjectively judged to be within the realm of reasonable expectation. An example is shown in Fig. 8.

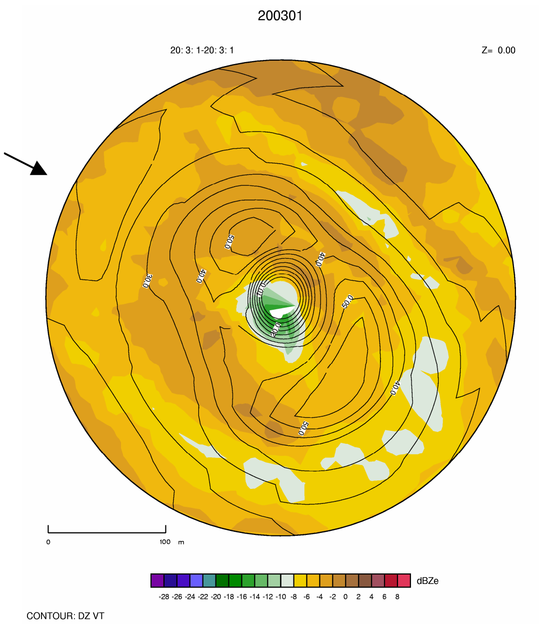

Fig. 6. Vortex-centered GBVTD analysis of the Doppler radar reflectivity field (filled color contours) and total azimuthal wind (contours of 5 m s^{-1}) for the sector scan taken at 20:03:01 CDT, when the tornado was at peak intensity. This scan contains azimuthal winds in excess of 50 m s^{-1} with a pronounced wavenumber-2 component (two diametrically opposed lobes of relatively high velocity just outside the tornado eye). The direction of the radar beam is indicated by the arrow.

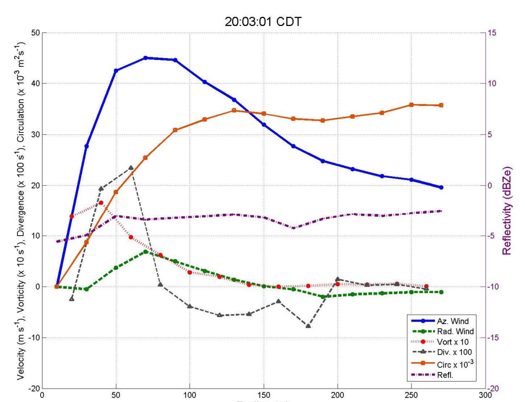

Fig. 7. Radial profile of GBVTD-analyzed azimuthally averaged azimuthal velocity (m s^{-1}), radial velocity (m s^{-1}), vorticity (s^{-1} x 10), divergence (s^{-1} x 100), circulation (m^2 s^{-1} x 10^{-3}), and reflectivity (dBZ_e) at 20:03:01 CDT. Positive radial velocity indicates flow away from the tornado vortex center.

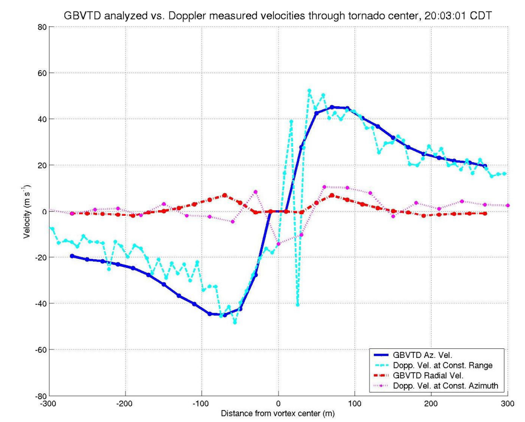

Fig. 8. GBVTD-analyzed wavenumber-0 (axisymmetric) azimuthal (solid line) and radial (dot-dash line) winds, and Doppler-measured along-beam velocities measured across the tornado vortex (dashed line) and along the radial passing through the center of the tornado vortex (dotted line) for the sector scan taken at 20:03:01 CDT.

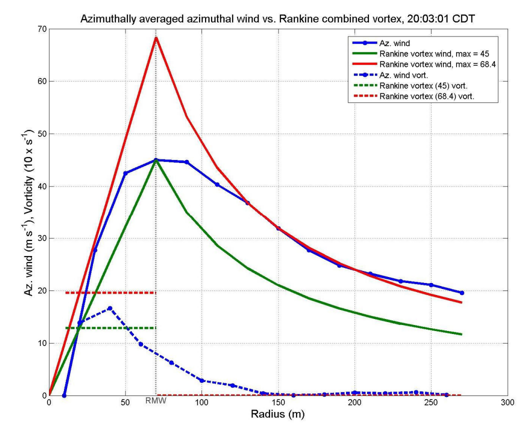

Fig. 9. Radial profile of GBVTD-analyzed azimuthally averaged azimuthal velocity from 20:03:01 CDT (solid blue curve), the azimuthal velocity profile of a Rankine combined vortex with the same maximum velocity value and RMW (solid green curve), the azimuthal velocity profile of a Rankine combined vortex with a best fit maximum value of 68.4 m s^{-1} (solid red curve). The vorticity profiles associated with each of the velocity profiles (multiplied by a factor of 10 for clarity) are indicated by broken lines with corresponding colors.

The intensity of the tornado, as measured by the maximum azimuthally averaged azimuthal wind speed, reached a peak of 45 m s^{-1} in the scan taken at 20:03:01 CDT. The radial profile of azimuthal velocity for this scan bore a strong resemblance to a Rankine vortex (blue curve,

Fig. 7). Within about 60 m from the center, the azimuthally averaged radial wind component increased with distance from the center, indicating divergence and sinking motion aloft. Between 60 m and 175 m, the azimuthally averaged radial wind component decreased with distance from the center, indicating convergence and rising motion aloft. The vortex thus looked like a two-celled vortex (Sullivan 1959), with sinking motion near the center and rising motion near the radius of maximum wind (RMW). The azimuthally averaged azimuthal wind then quickly decreased over the next three minutes as the tornado dissipated (Fig. 10).

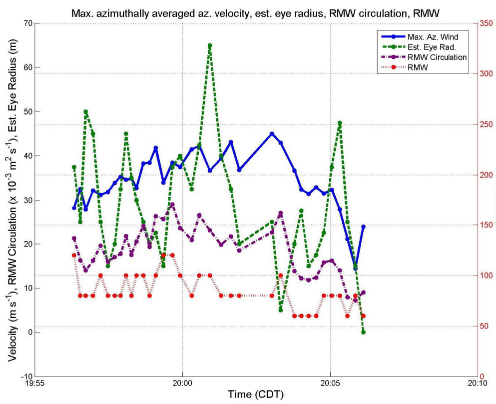

Fig. 10. Maximum azimuthally averaged azimuthal velocity, RMW, and estimated eye radius of the Stockton tornado as functions of time.

A plot of the estimated RMW, taken here as the radius of maximum azimuthally averaged azimuthal velocity as computed by the GBVTD technique, is also shown in Fig. 10. The RMW exhibited a general tendency to decrease with time. This behavior stands in contrast to the decay mode described by Bluestein *et al.* (2003) in the 5 June 1999 Bassett, Nebraska tornado, in which the RMW increased as the average azimuthal winds decreased.

Fig. 11 shows the evolution of the azimuthally averaged azimuthal wind structure as a function of time and radius. The maximum azimuthally averaged azimuthal wind increased in both magnitude and radius as the tornado proceeded through its life cycle, and displayed good temporal continuity until the tornado began to decay around 20:04:00 CDT. This decay phase coincided with a decrease in circulation of the wavenumber-0 component of the azimuthal wind at all radii (not shown).

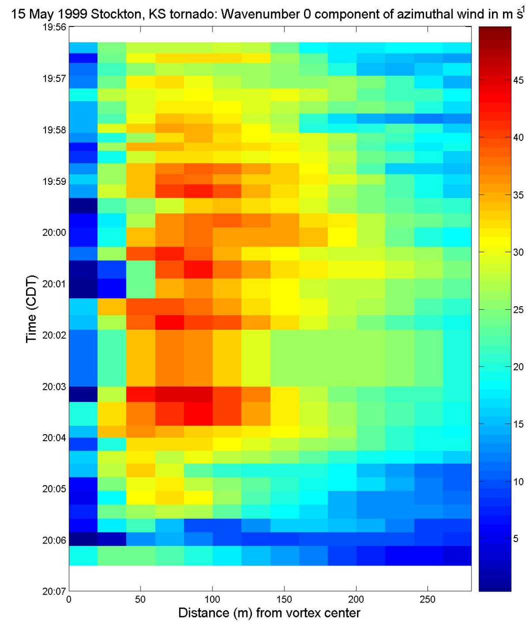

Fig. 11. Hovmoeller diagram of the azimuthally averaged wavenumber 0 component of the azimuthal (tangential) wind as a function of radius in the 15 June 1999 Stockton, Kansas tornado, as computed by the GBVTD analysis. The diameter of the eye approached 50 m around 20:01 CDT. Tornado threshold velocity is 35 m s^{-1}.

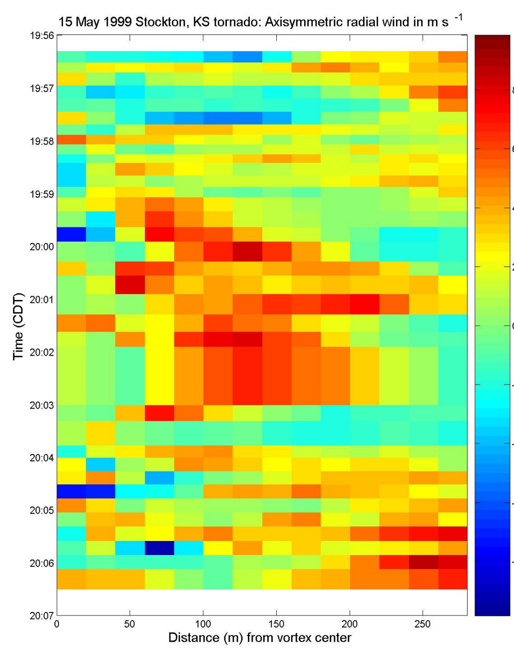

Fig. 12. Hovmoeller diagram of the axisymmetric component of the radial wind in the 15 May 1999 Stockton, Kansas tornado, as computed by the GBVTD analysis. The strongest outflow (positive radial velocity) occured when the tornado was ramping up to its peak intensity.

The GBVTD analyses also yielded azimuthally averaged radial profiles of higher order angular harmonics of the azimuthal wind (wavenumbers-1, -2, and -3). All three of these components (not shown) display poor temporal continuity and are of little value for interpretation. However, a relatively strong wavenumber-2 component of azimuthal velocity, manifest as two diametrically opposed “lobes” of relatively high values of analyzed azimuthal velocity, was readily apparent in 25 of the 35 scans, with a wavenumber-2 magnitude at or exceeding 5 m s^{-1}. These wavenumber-2 features exhibited poor temporal continuity in both magnitude and orientation.

6. INTERPRETATION

A number of significant temporal features of the Stockton tornado became apparent when several time-dependent variables were plotted on the same axis (Fig. 10). First, the low-reflectivity eye width decreased as the tornado approached its peak intensity (as measured by the maximum azimuthally averaged azimuthal wind) at 20:03:01 CDT, and then increased again as the tornado decayed. This fluctuation in eye width could be indicative of increased lofting of low-density debris particles (such as grass and dust) near the RMW as the intensity of the tornado increased (D. Burgess 2004, personal communication). Other arrhythmic fluctuations in eye width could result from the intermittent ingestion by the tornado of large quantities of small particles, which were then lofted to the level of the radar scan, (Bluestein *et al.* 2004).

Secondly, during the intensification period of the tornado (19:58:40 - 20:03:01 CDT), it can be seen that an increase in the maximum azimuthally averaged azimuthal wind at a relatively steady RMW resulted in an increase in circulation at the RMW. This manner of tornado intensification contrasts with that found by Bluestein *et al.* (2003) in their GBVTD analysis of the 5 June 1999 Bassett, Nebraska tornado (hereafter, “the Bassett tornado”). The RMW of the Bassett tornado decreased while the maximum azimuthally averaged azimuthal wind increased, and the circulation of the tornado at the RMW increased. This result suggests that more than one mode of tornado intensification exists.

Thirdly, it can be seen that as the tornado decreased in intensity towards the end of its life cycle (after 20:03:01 CDT), the RMW also generally decreased. This behavior contrasts markedly with the decay mode found by Bluestein *et al.* (2003) in the Bassett tornado. The Bassett tornado exhibited an increase in the RMW and a simultaneous decrease in maximum azimuthally averaged azimuthal wind. This result suggests that more than one mode of tornado decay exists.

The azimuthally averaged radial wind component of the tornado displayed a temporally coherent period of maximum outbound velocity (6 – 10 m s^{-1}) at roughly the same radii (60 – 120 m) and times (19:58:40 – 20:03:01 CDT) that the tornado was approaching its peak intensity (Fig. 12). Outflow from the tornado at the height of the scan, at these radii and times, is consistent with the two-celled vortex model. Outbound velocities from the center of the vortex may also be present at radii less than 60 m during this same time period as a result of contamination by centrifuging (Dowell *et al.* 2005). Dowell *et al.* (2005) assert that the velocities of centrifuged scatterers within a tornado may not be indicative of actual wind speeds inside of the tornado; however, this potential source of radial velocity (and hence, divergence) measurement error applies mainly to Doppler radar scans containing significant quantities of large scatterers, which were probably not present at the level of the radar scan (90 – 150 m) in the Stockton tornado. However, as previously noted, the GBVTD-analyzed values of azimuthally averaged radial velocity at radii less than 40 m should be considered somewhat suspect because relatively few velocity data points contributed to the GBVTD analysis.

As previously noted, a prominent wavenumber-2 component of azimuthal velocity was noted in the GBVTD analyses of 25 out of 35 scans. Previous GBVTD analyses of mobile radar data collected in tornadoes also exhibited a prominent wavenumber-2 component (Bluestein *et al.* 2003; Lee and Wurman 2005; W.-C. Lee 2004, personal communication). The reason for this feature is currently undetermined. It has been suggested that the wavenumber-2 component may be an artifact of the GBVTD analysis, or may in fact be a feature associated with tornadoes (Bluestein *et al.* 2003). The orientation of the wavenumber-2 feature does not appear to be correlated with the direction of the radar beam, nor does it exhibit continuity in magnitude or orientation from scan to scan. It is also unlikely that the wavenumber-2 feature is the result of aliasing from higher-order harmonics (wavenumber-4, wavenumber-6, etc.)

owing to the small contribution to the total azimuthal velocity component from the latter.

One possible physical explanation for the wavenumber-2 feature is that it is a result of the superposition of the horizontal vortex flow field and the horizontal deformation field associated with the inflow jet and gust front of the parent mesocyclone of the tornado. Yamauchi *et al.* (2002) demonstrated that vector addition of a deformation flow field and circular vortex flow yielded a flow pattern in which the vortex was deformed into an elliptically-shaped vortex with a strong wavenumber-2 component of velocity. In this case, the line connecting the two azimuthal velocity maxima is offset by 45° in the clockwise direction from the axis of dilatation of the deformation flow field. Curiously, in GBVTD analysis of such a flow pattern, the deformation flow field is aliased into wavenumber-1, not wavenumber-2 (M. Bell 2005, personal communication).

Dual-Doppler analyses applied to previous radar datasets collected in the hook echo regions of tornadic (Dowell and Bluestein 2002; Wakimoto *et al.* 1998, 2003) and non-tornadic (Wakimoto and Cai 2000) supercells at elevations below 1 km display a consistent signature of a deformation field at a distance of approximately 5 km from the tornado vortex signature (or vorticity maximum; Fig. 13), with an asymptote of confluence displaced from the tornado in the direction approximately perpendicular and to the right of the mean vertical shear vector, when the tornado is in its mature phase. This deformation field, however, is generally too distant to influence the outcome of our GBVTD analyses, for which velocities were calculated out to a distance of 280 m from the center of the Stockton tornado. A second possible physical explanation for the wavenumber-2 feature is that it is a result of elliptical asymmetry of the tornado vortex caused by translational and frictional effects (Shapiro 1983).

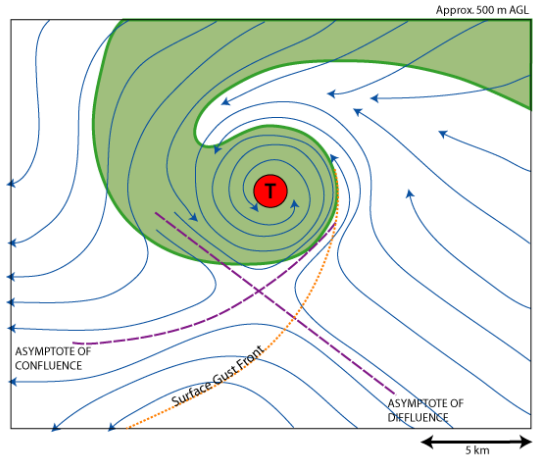

Fig. 13. Conceptual model of the hook echo region of a tornadic supercell (with a mature tornado) at an altitude of approximately 500 m AGL. The mesocyclone is partially occluded. The thin, unbroken lines with arrowheads represent the air flow trajectories at 500 m AGL; the gray region outlined by a thick, unbroken line represents a reflectivity contour of approximately 30 dBZ($_e$); the circled "T" represents the location of the tornado; the dotted line represents the approximate location of the surface gust front; and the dashed lines represent the asymptotes of diffluence and confluence (labeled). (*Note:* If the wind field were one of pure deformation, the asymptotes of confluence and diffluence would be considered the axes of dilatation and contraction, respectively.)

7. CONCLUSIONS

Application of the GBVTD analysis technique provided insight into the horizontal wind field in the 15 May 1999 Stockton, Kansas tornado, for which exceptionally high-quality W-band radar data were collected. From the GBVTD analysis, it can be inferred that the Stockton tornado probably possessed a two-celled structure during the period in which the tornado approached its peak intensity (19:58:40 – 20:03:01 CDT). Since no multiple vortices were visually observed during this period, vortex breakdown probably did not reach ground level at any time during the mature phase of the cycle of the tornado, when it could not have been detected at the altitude of the radar scan.

It can also be inferred from the results of the GBVTD analysis that the tornado wind field at the height of the radar scan resembled that of a Rankine-combined vortex during the period when the tornado approached its peak intensity. At the RMW, the transition from solid-body rotation in the inner region to potential flow in the outer region was analyzed as a gradual transition, possibly because the azimuthal velocity field of the tornado was probably not that of an ideal Rankine-combined vortex. The gradual transition may also have resulted from the smoothing inherent in the radar sampling, and from the GBVTD analysis technique as the reflectivity and velocity data were interpolated first from a radar-centered, polar PPI sector scan to a CAPPI grid in Cartesian coordinates, and then from the CAPPI grid to another polar grid centered around the vortex.

It can be seen from the radar data that the width of the low-reflectivity "eye" in the center of the tornado vortex fluctuated from scan to scan. Of particular interest is that the eye width decreased as the tornado approached its peak intensity at 20:03:01 CDT. One might expect that the width of the eye would increase with increasing tornado intensity as a result of increased centrifuging of scatterers (Dowell *et al.* 2005) and the horizontal divergence near the tornado core implied by the two-celled vortex structure previously discussed for this time period. It is noted that the eye width decreased again as the tornado decayed. These fluctuations could be indicative of increased ingestion and lofting of light debris inside the tornado, up to the altitude of the radar scan, as the intensity of the tornado increased.

From a comparison of the GBVTD analyses of the Stockton tornado and the Bassett tornado (Bluestein *et al.* 2003), it can be inferred that tornadoes exhibit two or more different modes of intensification and two or more different modes of decay. The RMW circulation in the Stockton tornado increased as a result of an increase of the maximum azimuthally averaged azimuthal velocity only; the RMW circulation in the Bassett tornado increased as a result of an increase of the maximum azimuthally averaged velocity that occurred along with a simultaneous decrease of the RMW. The RMW circulation of the Stockton tornado decreased as *both* the maximum azimuthally averaged azimuthal velocity and the RMW decreased; the RMW circulation of the Bassett tornado decreased as the maximum azimuthally averaged azimuthal velocity decreased and the RMW increased.

A significant wavenumber-2 component, with its amplitude at or exceeding 5 m s^{-1}, of the azimuthal wind was present in 25 out of 35 of the W-band sector scans. Similar wavenumber-2 features have been observed in previous studies in which the GBVTD analysis technique has been applied to mobile radar data collected in tornadoes. The presence of the wavenumber-2 feature in analyses of data collected by multiple radars (Lee and Wurman 2005; Bluestein *et al.* 2003) suggests that the wavenumber-2 feature may have a physical basis. It has been suggested that the wavenumber-2 feature may be result of the superposition of the vortex wind field upon a field of deformation as discussed by Yamauchi *et al.* (2002). Deformation flow fields have been shown to exist in close proximity to tornadoes in supercells, however, they usually are not present at a sufficiently small distance to directly influence the wind field around the tornado within the range at which the GBVTD analysis was applied.

Additional GBVTD analyses of mobile radar data collected in other tornadoes could provide a means of strengthening or disproving theories about tornado structure and evolution presented in this study and elsewhere. GBVTD analyses of data from radars with higher scan rates than the W-band radar could potentially clarify the source of the wavenumber-2 feature that has been repeatedly observed in mobile radar data collected in tornadoes. GBVTD analyses of data from radars that collect data at multiple elevation angles simultaneously (e.g., the rapid-scan Doppler on Wheels, or DOW5; Wurman and Randall 2001) and from dual-polarization radars (e. g. Lopez *et al.* 2004) could also potentially illuminate the structure of tornadoes.

8. ACKNOWLEDGMENTS

Stephan P. Nelson of the National Science Foundation (NSF) supported this project under NSF grant ATM-0241037. David C. Dowell of the National Severe Storms Laboratory (NSSL) furnished a copy of his video of the Stockton tornado for photogrammetric analysis.

9. REFERENCES

Bluestein, H. B., A. L. Pazmany, J. C. Galloway, and R. E. Mcintosh, 1995: Studies of the substructure of severe convective storms using a mobile 3-mm-wavelength Doppler radar. *Bull. Amer. Meteor. Soc.*. **76**, 2155 – 2170.

————, W.-C. Lee, M. Bell, C. C. Weiss, and A. L. Pazmany, 2003: Mobile Doppler radar observations of a tornado in a supercell near Bassett, Nebraska, on 5 June 1999. Part II: Tornado-vortex structure. *Mon. Wea. Rev.*, **131**, 2968 – 2984.

————, C. C. Weiss and A. L. Pazmany, 2004: Doppler radar observations of dust devils in Texas. *Mon. Wea. Rev.*, **132**, 209 – 224.

Doviak, R. J., and D. Sirmans, 1973. Doppler radar with polarization diversity. *J. Atm. Sci.*, **30**, 737 – 738.

Dowell, D. C., and H. B. Bluestein, 2002: The 8 June 1995 McLean, Texas, storm. Part I: Observations of cyclic tornadogenesis. *Mon. Wea. Rev.*, **130**, 2626 – 2648.

————, C. A. Alexander, J. Wurman, and L. J. Wicker, 2005: Centrifuging of hydrometeors and debris in tornadoes: Radar-reflectivity patterns and wind-measurement errors. *Mon. Wea. Rev.*, **133**, 1501 – 1524.

Lee, W.C., and F. D. Marks Jr., 2000. Tropical cyclone kinematic structure retrieved from single-Doppler radar observations. Part II: The GBVTD-Simplex center-finding algorithm. *Mon. Wea. Rev.*, **128**, 1925 – 1936.

————, and J. Wurman, 2005: Diagnosis of the 3-D axisymmetric structure of the Mulhall, Oklahoma tornado of 3 May 1999. *J. Atmos. Sci.*, **62**, 2373 – 2393.

————, F. D. Marks Jr., and R. E. Carbone, 1994: Velocity track display – A technique to extract real-time tropical cyclone circulations using a single airborne Doppler radar. *J. Atmos. Oceanic Technol.*, **11**, 337 – 356.

————, B. J.-D. Jou, P.-L. Chang, and S.-M. Deng, 1999: Tropical cyclone kinematic structure retrieved from single-Doppler radar observations. Part I: Doppler velocity patterns and the GBVTD technique. *Mon. Wea. Rev.*, **127**, 2419 – 2439.

————, B. J-.D. Jou, P.-L. Chang, and F. D. Marks Jr., 2000. Tropical cyclone kinematic structure retrieved from single-Doppler radar observations. Part III: Evolution and structures of Typhoon Alex. *Mon. Wea. Rev.*, **128**, 3982 – 4001.

Lopez, F. J., A. L. Pazmany, H. B. Bluestein, M. R. Kramar, M. F. French, C. C. Weiss, and S. Frasier, 2004: Dual-polarization, X-band, mobile Doppler radar observations of hook echoes in supercells. Preprints, *22nd Conf. on Severe Local Storms*, Hyannis, MA, Amer. Meteor. Soc., CD-ROM, P11.7.

Oye, R. C. K. Mueller, and S. Smith, 1995: Software for radar translation, editing, and interpolation. Preprints, *27th Conf. on Radar Meteorology*, Amer. Meteor. Soc., 359 – 361.

Pazmany, A. L., J. C. Galloway, J. B. Mead, I. Popstefanija, R. E. McIntosh and H. B. Bluestein, 1999: Polarization diversity pulse-pair technique for millimeter-wave Doppler radar measurements of severe storm features. *J. Atmos. Oceanic Technol.,* **16**, 1900 – 1911.

Shapiro, L. J., 1983: The asymmetric boundary layer flow under a translating hurricane. *J. Atm. Sci.*, **40**, 1984 – 1998.

Sullivan, R. D., 1959: A two-cell vortex solution of the Navier-Stokes equations. *J. Aerospace Sci.*, **26**, 767-768.

Wakimoto R. M., and H. Cai, 2000: Analysis of a nontornadic storm during VORTEX 95. *Mon. Wea. Rev.,* **128**, 565 – 592.

————, R. M., C. Liu and H. Cai, 1998: The Garden City, Kansas, storm during VORTEX 95. Part I: Overview of the storm's life cycle and mesocyclogenesis. *Mon. Wea. Rev.,* **126**, 372 – 392.

————, R. M., H. V. Murphey, D. C. Dowell and H. B. Bluestein, 2003: The Kellerville tornado during VORTEX: Damage survey and Doppler radar analyses. *Mon. Wea. Rev.,* **131**, 2197 – 2221.

Ward, N. B., 1972: The exploration of certain features of tornado dynamics using a laboratory model. *J. Atmos. Sci.,* **29**, 1194–1204.

Wood, V. T., and R. A. Brown, 1992: Effects on radar proximity on single-Doppler velocity signatures of axisymmetric rotation and divergence. *Mon. Wea. Rev.*, **120**, 2798-2807.

————, and ————, 1997: Effects of radar sampling on single-Doppler velocity signatures of mesocyclones and tornadoes. *Wea. Forecasting*, **12**, 928 – 938.

Wurman, J., and M. Randall, 2001: An inexpensive, mobile, rapid-scan radar. Preprints, *30th Conf. on Radar Meteorology*, Munich, Germany, Amer. Meteor. Soc., CD-ROM, P3.4.

Yamauchi, H., O. Suzuki, and K. Akeada, 2002: Asymmetry in wind field of Typhoon 0115 analyzed by triple Doppler radar observations. Preprints, *Int. Conf. on Mesoscale Convective Systems and Heavy Rainfall/Snowfall in East Asia*. Tokyo, Japan, Japan Science and Technology Corporation and Chinese Academy of Meteorological Sciences, 245 – 250.